

# Exploring the Free Energy Landscape: From Dynamics to Networks and Back

Diego Prada-Gracia<sup>1,2</sup>, Jesús Gómez-Gardeñes<sup>2,3</sup>, Pablo Echenique<sup>2,4</sup>, Fernando Falo<sup>1,2,\*</sup>

**1** Departamento de Física de la Materia Condensada, Universidad de Zaragoza, E-50009 Zaragoza, Spain

**2** Instituto de Biocomputación y Física de Sistemas Complejos (BIFI), Universidad de Zaragoza, E-50009 Zaragoza, Spain

**3** Departamento de Matemática Aplicada, ESCET, Universidad Rey Juan Carlos, E-28933 Móstoles (Madrid), Spain

**4** Departamento de Física Teórica, Universidad de Zaragoza, E-50009 Zaragoza, Spain

\* E-mail: fff@unizar.es

## Abstract

The knowledge of the Free Energy Landscape topology is the essential key to understand many biochemical processes. The determination of the conformers of a protein and their basins of attraction takes a central role for studying molecular isomerization reactions. In this work, we present a novel framework to unveil the features of a Free Energy Landscape answering questions such as how many meta-stable conformers are, how the hierarchical relationship among them is, or what the structure and kinetics of the transition paths are. Exploring the landscape by molecular dynamics simulations, the microscopic data of the trajectory are encoded into a Conformational Markov Network. The structure of this graph reveals the regions of the conformational space corresponding to the basins of attraction. In addition, handling the Conformational Markov Network, relevant kinetic magnitudes as dwell times and rate constants, or hierarchical relationships among basins, complete the global picture of the landscape. We show the power of the analysis studying a toy model of a funnel-like potential and computing efficiently the conformers of a short peptide, the dialanine, paving the way to a systematic study of the Free Energy Landscape in large peptides.

## Author Summary

A complete description of complex polymers, such as proteins, includes information about their structure and their dynamics. In particular it is of utmost importance to answer the following questions: What are the structural conformations possible? Is there any relevant hierarchy among these conformers? What are the transition paths between them? These and other questions can be addressed by analyzing in an efficient way the Free Energy Landscape of the system. With this knowledge, several problems about biomolecular reactions (such as enzymatic activity, protein folding, protein deposition diseases, etc) can be tackled. In this article we show how to efficiently describe the Free Energy Landscape for small and large peptides. By mapping the trajectories of molecular dynamics simulations into a graph (the Conformational Markov Network), and unveiling its structural organization, we obtain a coarse grained description of the protein dynamics across the Free Energy Landscape in terms of the relevant kinetic magnitudes of the system. Therefore, we show the way to bridge the gap between the microscopic dynamics to the macroscopic kinetics by means of a mesoscopic description of the associated Conformational Markov Network. Along this path the compromise between the physical nature of the process and the magnitudes that characterize the network is carefully kept to assure the reliability of the results shown.

## Introduction

Polymers and, more specifically, proteins, show complex behavior at the cellular system level, *e.g.* in protein-protein interaction networks [1], and also at the individual level, where proteins show a large degree of multistability: a single protein can fold in different conformational states [2–4]. As a complex system [5, 6], the dynamics of a protein cannot be understood by studying its parts in isolation, instead, the system must be analyzed as a whole. Tools able to represent and handle the information of the entire picture of a complex system are thus necessary.

Complex network theory [7, 8] has proved to be a powerful tool used in seemingly different biologically-related fields such as the study of metabolic reactions, ecological and food webs, genetic regulatory systems and the study of protein dynamics [7]. In this latter context, diverse studies have analyzed the conformational space of polymers and proteins making use of network representations [9–12], where nodes account of polymer conformations. Additionally, some studies have tried to determine the common and general properties of these conformational networks [13, 14] looking at magnitudes such as clustering coefficient, cyclomatic number, connectivity, etc. Recently, trying to decompose the network in modules corresponding to the free energy basins, the use of community algorithms over these conformational networks have been proposed [15]. Although this approach has opened a promising path for the analysis of Free Energy Landscapes (FEL), the community based description of the network leads to multiple characterizations of the FEL and thus it is difficult to establish a clear map from the communities found to the basins of the FEL.

A similar approach, commonly used to analyze the complex dynamics, is the construction of Markovian models. Markovian state models let us treat the information of one or several trajectories of molecular dynamics (MD) as a set of conformations with certain transition probabilities among them [9, 16, 17]. Therefore, the time-continuous trajectory turns into a transition matrix, offering global observables as relaxation times and modes. In [16–18] the use of Markovian models is proposed with the aim of detecting FEL meta-stable states. However, the above approaches to analyze FELs of peptides involves extremely large computational cost: either general community algorithms or large transition matrices.

Finally, other strategies to characterize the FEL that have successfully helped to understand the physics of biopolymers, are based on the study of the Potential Energy Surface (PES) [3, 4, 19–21]. The classical transition-state theory [22] allows us to project the behavior of the system at certain temperature from the knowledge of the minima and transition states of the PES. This approach entails some feasible approximations, such as harmonic approximation to the PES, limit of high damping, assumption of high barriers, etc. These approximations could be avoided working directly from the MD data.

In this article we make a novel study of the FEL capturing its mesoscopic structure and hence characterizing conformational states and the transitions between them. Inspired by the approaches presented in [12, 15] and [16, 17], we translate a dynamical trajectory obtained by MD simulations into a Conformational Markov Network. We show how to efficiently handle the graph to obtain, through its topology, the main features of the landscape: conformers and their basins of attraction, dwell times, rate constants between the conformational states detected and a coarse-grained picture of the FEL. The framework is shown and validated analyzing a synthetic funnel-like potential. After this, the terminally blocked alanine peptide (Ace-Ala-Nme) is studied unveiling the main characteristics of its FEL.

## Methods

In this section we show the round way of the FEL analysis: the map of microscopic data of a MD into a Conformational Markov Network (CMN) and, by unveiling its mesoscopic structure, the description of the FEL structure in terms of macroscopic observables.

## Translating the FEL into a network

First, we encode a trajectory of a stochastic MD simulation into a network: the CMN. This map will allow us to use the tools introduced henceforth to analyze a specific dynamics of complex systems such as biopolymers.

### Conformational Markov Network

The CMN has been proven to be a useful representation of large stochastic trajectories [10, 11, 15]. This coarse grained picture is usually constructed by discretizing the conformational space explored by the dynamical system and considering the hops between the different configurations as dictated by the MD simulation. In this way, the nodes of a CMN are the subsets of configurations defined by the conformational space discretization and the links between nodes account for the observed transitions between them. The information of the stochastic trajectory allows to assign probabilities for the occupation of a node and for the transitions between two different configurations. Defined as above, a CMN is thus a weighted and directed graph.

Our CMN is constructed as follows. The conformational space is divided into  $N$  cells of equal volume, therefore every node  $i$  ( $i = 1, \dots, N$ ) of the CMN contains the same number of possible configurations. Next, by evolving a stochastic trajectory enough time steps (of length  $\Delta t$ ) to assure the ergodicity condition we can define the final CMN set up. We assign to each node a weight,  $P_i$ , that accounts for the fraction of trajectory that the system has visited any of the configurations contained in node  $i$  (the following normalization  $\sum_i P_i = 1$  holds). Second, a value  $P_{ij}$  is assigned to each directional link, accounting for the number of hops from node  $j$  to node  $i$ . Note that transitions between configurations contained in the same node are also considered by  $P_{ii}$ , *i.e.* the network can also contain self-loops. Finally, the weights of the outgoing links from a node  $j$ ,  $\{P_{ij}\}$ , are conveniently normalized so that  $\sum_i P_{ij} = 1$ .

The CMN constructed in this way, is described by a single matrix  $\mathbf{S} = \{P_{ij}\}$  and a vector whose components are the occupation probabilities  $\vec{P} = \{P_i\}$ . Hence, the matrix  $\mathbf{S}$  is the transition probability matrix of the following Markov chain,

$$\vec{v}(t + \Delta t) = \mathbf{S}\vec{v}(t) \quad (1)$$

where  $\vec{v}(t)$  is the instant probability distribution of the system at time  $t$ . Since the matrix  $\mathbf{S}$  is ergodic and time invariant, one can compute the stationary distribution associated to the Markov chain,  $\vec{v}^e$ , that satisfies  $\vec{v}^e = \mathbf{S}\vec{v}^e$ . The latter stationary distribution has to be identical to the computed weights of the network nodes,  $P_i = v_i^e$  ( $i = 1, \dots, N$ ), provided the stochastic trajectory is long enough. Moreover, the detailed balance condition,

$$P_{ji}P_i = P_{ij}P_j \quad (2)$$

must hold thus relating the elements of matrix  $\mathbf{S}$  to the stationary probability distribution. Therefore, the transition matrix  $\mathbf{S}$  appears to be the minimal descriptor of the stochastic trajectory and, as consequence, of the CMN.

### Markovity

Provided the MD trajectory is long enough to consider the sample in equilibrium, the weight-distribution of nodes in the CMN will be the stationary solution of Eq. (1) and detailed balance condition (2) will be fulfilled [23]. However, this property is not enough to consider the model Markovian: Although the continuous trajectory will be produced using Langevin dynamics (and therefore inherently Markovian in the phase space [24, 25]) the discrete representation of the CMN and the integration of momenta defies the Markovian character of our model [24, 26–28]. Several methods are proposed in the literature to validate Markov models [16, 27, 29]. In order to obtain a reliable description, specially about those magnitudes related to the time evolution of the system (see subsection Temporal hierarchy of basins), the time step  $\Delta t$  must be large enough to avoid memory effects [27].

A detailed check and discussion about the Markovian character of the networks shown in this article can be found in the *Supporting Information Text (SI)*.

### Funnel-like potential

To illustrate the CMN approach and the methods presented below, we introduce here a synthetic potential energy function, that serve us as a toy model where results can be easily interpreted. This potential energy is reminiscent of that funnel surfaces recurrently found when the FEL of proteins are studied [30,31]. In particular, we have considered a two-dimensional system where a particle moves in contact with a thermal reservoir and whose potential energy is given by,

$$V(x, y) = \frac{1}{2}(x^2 + y^2) - (a_0 + a_1 \sin(b_1 x) + a_2 \sin(b_2 x) + a_3 \sin(b_3 y))e^{-\frac{1}{2}(x^2 + y^2)}, \quad (3)$$

where we have set  $a_0 = 4$ ,  $a_1 = 1.6$ ,  $a_2 = 0.8$ ,  $a_3 = 1.2$ ,  $b_1 = 6$ ,  $b_2 = 15$  and  $b_3 = 6$ . As shown in Figure 1A the above potential energy confines the movement of the stochastic trajectory inside a finite region of the conformational space. However, thermal fluctuations allow the particle to jump between several basins of attraction.

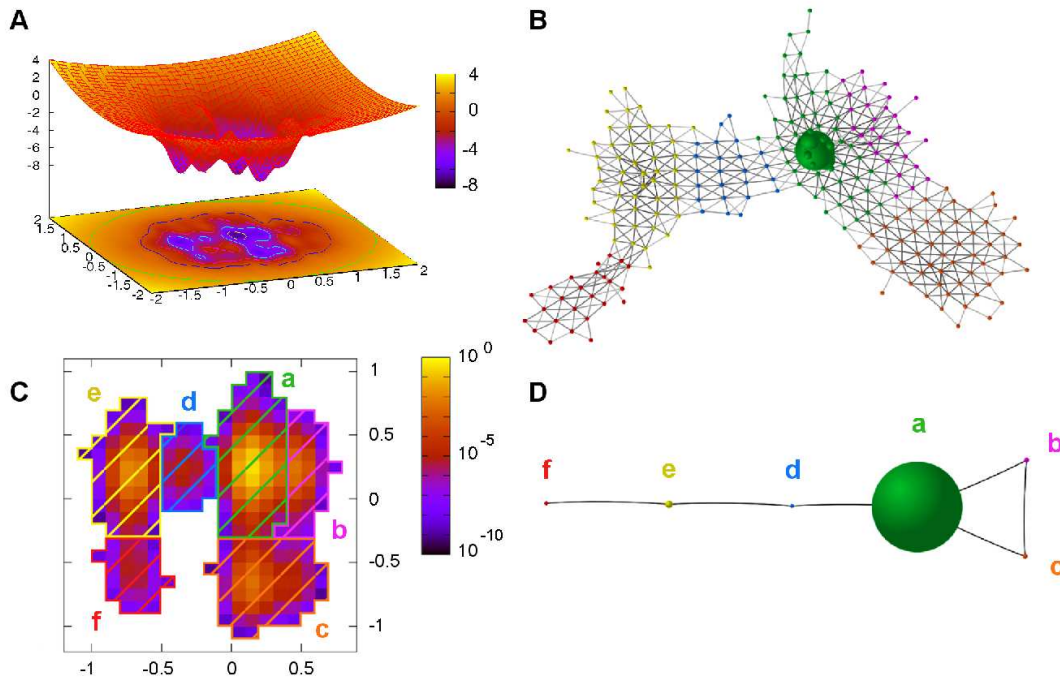


**Figure 1. SSD algorithm applied to a synthetic funnel-like potential.** (A) 2D funnel-like potential. (B) A stochastic trajectory is translated into a CMN where 6 sets of nodes (corresponding to different color) are the result of the SSD algorithm. (C) Recovering the spatial coordinates, the stationary probabilities of each node are shown in color code. The 6 basins detected are represented as color striped regions. (D) A coarse-grained CMN is built where new nodes take the role of the basins.

A stochastic trajectory has been simulated using an overdamped Langevin dynamics and the equations of motion have been integrated with a fourth order stochastic Runge-Kutta method [32]. Figure 1C shows the region of the conformational space visited by the particle. We have conveniently discretized the two-dimensional space into pixels of equal area and computed their corresponding occupation probabilities. Thereby, with the transition probabilities between pixels, the trajectory is represented as the CMN shown in Figure 1B. The question now is: can we recover the topology of the FEL (derived from Eq. (3)) from the CMN representation?

## Analyzing the FEL through the network

Up to now, we have illustrated the conversion of molecular dynamics data into a graph (the CMN). Now, we show how to efficiently obtain the thermo-statistical data from the mesoscopic description of the CMN.

### Revealing structure: conformational basins

Inspired by the deterministic steepest descent algorithm to locate minima in a potential energy surface we propose a *Stochastic Steepest Descent* (SSD) algorithm to define basins on the discretized FEL. Dealing with the nodes and links as we describe below, the proper structure of the CMN is unveiled to call the modules obtained conformational macro-states or basins.

Picking at random one node of the CMN, say  $a$ , and an initial probability distribution  $P_i(0) = \delta_{i,a}$  ( $i = 1, \dots, N$ ), the Markov process relaxes according to  $\vec{P}(\Delta t) = \mathbf{S}\vec{P}(0)$ . The whole probability concentrated in node  $a$  at time 0, in a single time step  $\Delta t$ , evolves driving the maximum amount of probability down hill over the FEL. The next node  $b$  in the descendent pathway from  $a$  is taken by following the link that carries maximum probability flux. Focusing again all the probability in node  $b$ ,  $P_i(1) = \delta_{i,b}$  we continue the pathway from  $a$  towards a local FEL minimum by identifying the next node  $c$  for which the probability current  $P_{c,b}$  is maximal. Iterating this operation for each node of the CMN, we obtain a set of disconnected descent pathways that help us to define the basins of attraction.

We establish formally the above procedure assisted by a vector  $\vec{\Omega} = \{\omega_i\}$  (with  $i = 1, \dots, N$ ) that label the nodes:

- (i) We start by assigning  $\vec{\Omega} = \vec{0}$ .
- (ii) Select at random a node  $l$  with  $\omega_l = 0$  (*i.e.*,  $l$  has not been labeled yet) and start to write an auxiliary list  $V$  of nodes adding  $l$  as the first entry in this list.
- (iii) Search, within the neighbors of the node  $l$ , a node  $m$  so that  $P_{ml} = \max\{P_{j,l}, \forall j \neq l\}$  [33] and check which of the following options is fulfilled:
  - A If  $P_{ml} > P_{lm}$  and  $\omega_m = 0$ : add  $m$  to the list  $V$  and go again to (iii) taking  $m$  in the place of  $l$ .
  - B If  $P_{ml} > P_{lm}$  and  $\omega_m \neq 0$  then write the labels of all the nodes in the list  $V$  as  $\omega_j = \omega_m \forall j \in V$ . The process continues going to step (ii).
  - C If  $P_{ml} \leq P_{lm}$  the link  $l \rightarrow m$  is removed from the graph. The process returns to step (iii) with the next exception: since this step has been iterated  $2D$  times for the same node  $l$  (being  $D$  the number of coordinates discretized to construct the CMN),  $l$  is stated as local minimum and  $\omega_l = l$ . In this case  $\omega_j = l$  for those nodes  $j \in V$  and the process comes back to step (ii).

The whole procedure ends when no nodes unlabeled remain in the CMN,  $\omega_i \neq 0 \forall i$ . The restriction introduced in step (iii.C) with the dimensionality  $D$  avoids a transition from a local minimal energy configuration to any other node of the same basin or to a deeper local minimum of a different basin. When every node of the CMN has been visited, the conformational space is completely characterized and

we have thus traced all the maximum descent pathways from any node to the local FEL minima. Finally, all those nodes with the same label  $\omega_i$  belong to the same FEL basin and therefore they are associated to the same conformational state. The result of the procedure is the partition of the CMN in a set of modules which correspond to basins of attraction of the discretized conformational space.

To illustrate the basin decomposition of a CMN, the SSD algorithm has been applied to the funnel-like potential. The result is the detection of six basins in agreement with the number of local minima in its FEL (Figure 1B and 1C).

### Comparing with other community algorithms

With the aim of studying biomolecules and systems with high degree of dimensionality, the way to detect these FEL basins must be computationally efficient. The method described above takes a computational time  $\mathcal{O}(2DN)$ , once the  $2D$  largest hooping probabilities  $P_{ji}$  are computed for all the nodes in the network. Additionally, the method is deterministic providing with a unique partition of the CMN into different modules. These two characteristics make this analysis faster and more straightforward than any other partitioning method [34]. These advantages come from the knowledge of the physical meaning of links and nodes of CMNs. In the *SI* other community algorithms (Newman’s modularity and Markov Clustering algorithm) are tested over our toy model system. None of the algorithms reported in the *SI* give a satisfactory result mapping the modules obtained with the free energy basins.

### Coarse-Grained CMN

To get a more comprehensible representation of the FEL studied, a new CMN network can be built by taking the basins as nodes. The occupation probabilities of these nodes as well as the transition probabilities among them can be obtained from those of the original CMN as

$$P_\alpha = \sum_{i \in \alpha} P_i, \quad (4)$$

$$P_{\beta\alpha} = \frac{\sum_{i \in \alpha} \sum_{j \in \beta} P_{ji} P_i}{\sum_{i \in \alpha} P_i}, \quad (5)$$

where  $i$  and  $j$  are indexes relative to the nodes of the original CMN and  $\alpha$  and  $\beta$  are indexes for the basins (new nodes). Note that the new coarse-grained CMN has its weights normalized and fulfills the detailed balance condition Eq. (2). Figure 1D shows the corresponding coarse-grained for the funnel-like potential.

The weighted nodes and links have a clear physical meaning [19]. Considering the transition state  $\alpha \rightarrow \beta$  and assuming local "intra-basin" equilibrium, the rate constant of this transition is  $k_{\alpha\beta} = P_{\beta\alpha}/\Delta t$  (where  $\Delta t$  is the time interval between snapshots used to make the original CMN). The relative free energy of the basin  $\alpha$ , taking basin  $\beta$  as reference, is  $\Delta F_\alpha = -k_B T \log(P_\alpha/P_\beta)$ . Besides, the expected waiting time to escape from  $\alpha$  to any adjacent basin is  $\tau_\alpha = \Delta t/(1 - P_{\alpha\alpha})$  [35]. Other magnitudes, such as first-passage time for inter-basins transitions and other rate constants relaxing the local equilibrium condition [19, 35] can also be computed from the original CMN.

The ability to define the proper regions of the conformational space in an efficient way let us compute physical magnitudes of relevance. For instance, the coarse-grained CMN is nothing but a graphical representation of a kinetic model with  $n$  (the number of basins) coupled differential equations:

$$\frac{dP_\alpha(t)}{dt} = - \sum_{\beta \neq \alpha} k_{\beta\alpha} P_\alpha(t) + \sum_{\beta \neq \alpha} k_{\alpha\beta} P_\beta(t). \quad (6)$$



### Free Energy hierarchical basin organization

The first hierarchy aims to answer the following question: What is the structure of the CMN when nodes with lower weight than a certain threshold are removed together with their links? Let us take the control parameter  $F/k_B T$  as the threshold to restrict the existence of the nodes in the original CMN. Where  $F_i/k_B T = \log(P_w) - \log(P_i)$  is the “*adimensional free energy*” of a node  $i$  relative to the most weighted node  $w$ .

With the above definitions we start a CMN reconstruction by smoothly increasing the threshold from its zero value. At each step of this process, we obtain a network composed of those nodes with free energy lower than the current threshold value. As the free-energy cut-off increases, new nodes emerge together with their links. These new nodes may be attached to any of the nodes already present in the network or they can emerge as a disconnected component. At a certain value of  $F/k_B T$ , some components of the network become connected by the links of a new node incorporated at this step. A Hoshen-Kopelman like algorithm [36] is used to detect the disconnected components of the network at each value of the

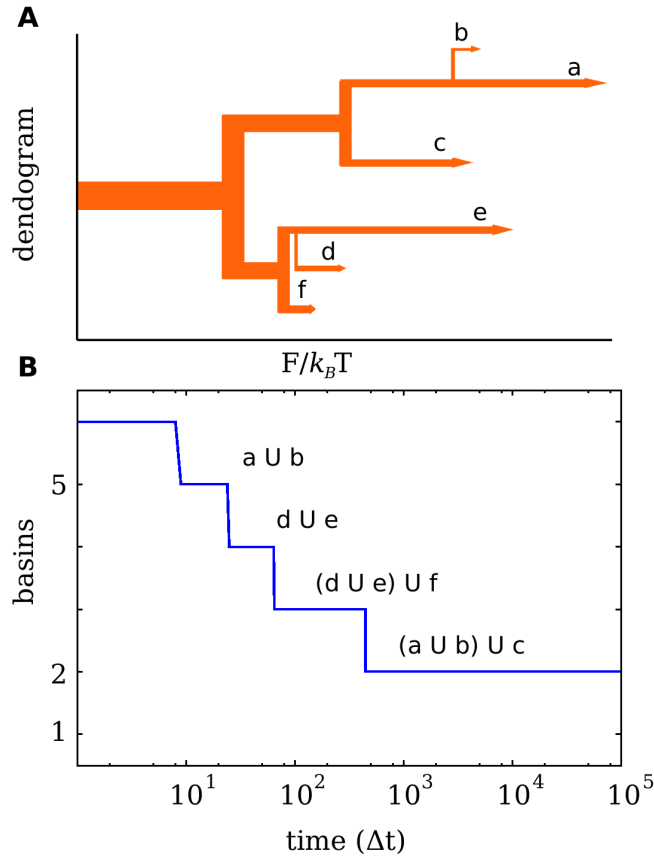


**Figure 2. Hierarchies of the basins detected for the funnel-like potential.** (a) Free Energy hierarchy: based on the relative free-energy of the nodes. (b) Temporal hierarchy: number of basins defined by SSD for the different networks built by eq. (7). The original basins merge in function of time. Both hierarchies reveals a coarse-grained behavior of two macro-states:  $(a \cup b \cup c)$  and  $(d \cup e \cup f)$ .

threshold used: from zero until all the  $N$  nodes of the CMN were already attached.

This bottom-up network reconstruction provides us with a hierarchical emergence of nodes along with the way they join together. This picture can be better described by a process of basins emergence and linking that is easily represented by means of a basin dendogram. This representation let us guess at first glance the hierarchical relationship of the conformational macro-states and the height of the barriers between them. Let us remark that the transition times cannot be deduced from these qualitative barriers since the entropic contribution or the volume of the basin are not reflected in this diagram. The basins family-tree obtained for the funnel-like (see Figure 2A) reveals that, despite of having a two-dimensional potential with the shape of a funnel, one cannot describe it as a sequence of metastable conformations that drive the system to the global minimum. Moreover, the diagram shows a roughly similar behavior as for a double asymmetric well, composed by two sets of basins:  $(a \cup b \cup c)$  and  $(d \cup e \cup f)$ .

### Temporal hierarchy of basins

The CMN representation of a MD simulation provides with another hierarchical relationship that is meaningful to understand the behavior of the biological systems. The links of the original CMN have been weighted according to the stochastic matrix  $\mathbf{S} = \{P_{ij}\}$ . Taking into account the Markovian character of the process, we can make use of the Chapman-Kolmogorov equation to generate new transition matrices at times  $\tau = 2\Delta t, 3\Delta t, \text{etc.}$  Formally, the Markov chain at sampling time  $m\Delta t$  is defined by the matrix:

$$\mathbf{S}(m\Delta t) = [\mathbf{S}(\Delta t)]^m . \quad (7)$$

For each value of  $m$  a new CMN is defined. This family of CMNs have different weighted links but the same weights  $P_i$  for the nodes as the original one ( $m = 1$ ). It is worth to discuss the behavior of the matrix  $\mathbf{S}(m\Delta t)$ . In the limit  $m \rightarrow \infty$  we have  $\vec{P} = \mathbf{S}(m\Delta t)\vec{P}(0)$ , independently of the initial state  $\vec{P}(0)$ . This means that any node is connected to a given node of the network with the same weight, regardless of the initial source. Therefore, only one basin would be detected by the SSD algorithm since every node is connected with the most weighted link to the most weighted node in only one step.

From the original  $\Delta t$ -description of the FEL to the integrated ( $m\Delta t \rightarrow \infty$ ) one, we can devise another algorithm to establish a second hierarchy of the basins by performing the next two operations: First, for each value of  $m$  a new CMN is generated by constructing the matrix  $[\mathbf{S}(\Delta t)]^m$  and second, the SSD algorithm is applied to this new CMN. The process finishes when only a basin (the whole network) is detected (for large enough values of  $m$ ). By using this technique we can observe how basins merge with others at different time scales (labeled by the integer  $m$ ).

The result of this procedure performed for the funnel-like potential is shown in Figure 2B. At  $\tau \approx 500$  only two basins are observed:  $(a \cup b \cup c)$  and  $(d \cup e \cup f)$ , being the largest plateau observed for any of the nontrivial arrangement of basins found. Therefore, the macroscopic description in time is in agreement with the Free Energy hierarchy described previously. It is clear that the number of basins decrease as  $m$  increases. One should be aware that the concept of basin depends dramatically on the time resolution at which the CMN is built, and this time limits also the resolution in the FEL structure. Note also that this procedure provides with useful information similar to the *structural decorrelation time* [37].

## Results

### The Alanine dipeptide.

The alanine dipeptide, or terminally blocked alanine peptide (Ace-Ala-Nme, Figure 3A), is the most simple "biological molecule" that exhibits the common features shown by larger biomolecules. Despite of its simplicity, this system has more than one long-life conformational state with different transition



pathways. Since the first attempt by Rossky and Karplus [38] to model this dipeptide solvated, this system has been widely studied in theoretical works [39–42]. The alanine dipeptide has been also the appropriate molecule to test tools to explore the FEL [15, 16, 43] and, specifically, to study reaction coordinates [42, 44].

The alanine dipeptide has two slow degrees of freedom, the rotatable bonds  $\phi$  (C-N-C $_{\alpha}$ -C) and  $\psi$  (N-C $_{\alpha}$ -C-N) (see Figure 3A). The FEL projected onto these dihedral angles let us identify the conformational states that characterize the geometry of biopolymers, namely: alpha helix right-handed ( $\alpha_R$ ), alpha helix left-handed ( $\alpha_L$ ), beta strands ( $C_{7eq}, C_5$ ), etc. The number of local minima in the ( $\phi, \psi$ ) space depends on the effective potential model used to simulate the system. Up to date, electronic structure calculations have identified a total of nine different conformers [45]. Regarding MD simulations different conformational states have been observed: (i) using classical force fields with explicit solvent up to six conformers are detected [16, 39, 40], (ii) at least four stable states by using implicit solvent [15, 39, 41], and (iii) two stable conformers in vacuum conditions [39, 42]. On the other hand, since the angles  $\phi$

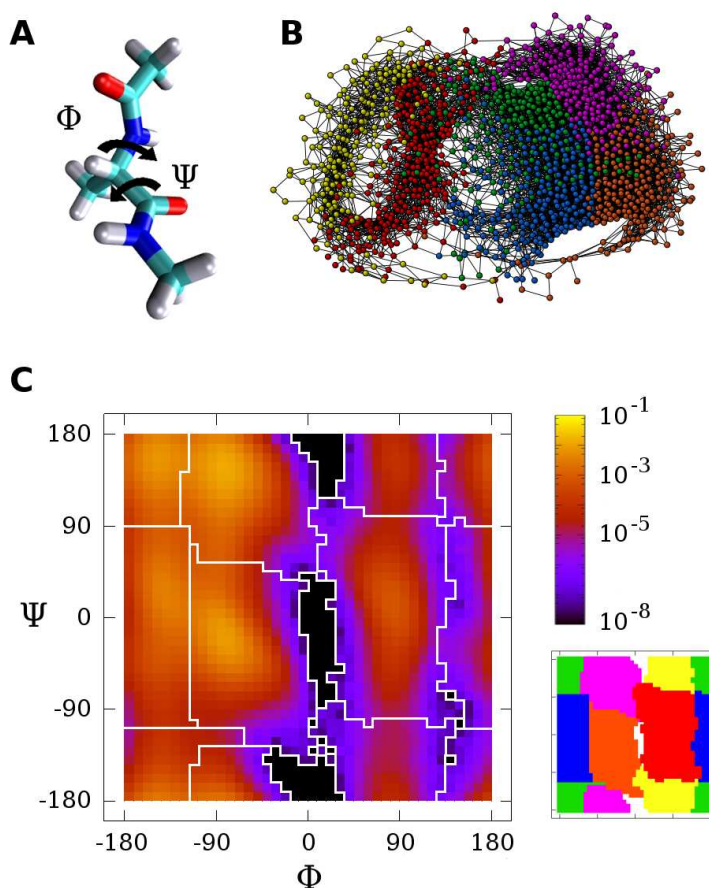


**Figure 3. Free energy basins of the Alanine dipeptide.**(A) The dialanine dipeptide with the angles  $\phi$  and  $\psi$ . (B) Plot of the CMN generated. The 6 sets of nodes (corresponding to different colors) are the result of the SSD algorithm. (C) Left: Ramachandran plot with the probability of occupation of the cells used to build the CMN. The boundaries of the free energy basins are shown in white. Right: the 6 basins represented as regions of different color. (Color code: orange =  $\alpha_R$ , red =  $\alpha_L$ , yellow =  $C_{7ax}$ , pink =  $C_{7eq}$ , green =  $C_5$  and blue =  $\alpha'$ ).

and  $\psi$  seem appropriate to distinguish the metastable states, the kinetics between them is not accurately described with this choice of reaction coordinates, the solvent coordinates and/or other internal degrees of freedom must be taken into account [42, 44].

We have used *SSD* algorithm to detect the local minima and their corresponding basins for this molecule in the  $\phi$ - $\psi$  space. For this purpose, a Langevin MD simulation of 250 ns has been performed at a temperature of 400 K (see the *SI* for further details). Additionally the CMN has been built dividing the  $(\phi, \psi)$  Ramachandran plot into cells of surface  $9^\circ \times 9^\circ$  ( $40 \times 40$ ) and taking dialanine conformations at time intervals of  $\Delta t = 0.01$  ps. The resulting CMN have a total of  $n = 1505$  nodes and  $e = 26324$  directed links.

The *SSD* algorithm applied to the CMN network reveals 6 basins. Figure 3B shows the resulting network where nodes belonging to the same basin take the same color. Bringing back this information to the Ramachandran map, these 6 sets of nodes define 6 regions represented in Figure 3C. To better illustrate this division, other representation, where each region has a different color, is shown. By comparing with previous studies on this molecule, we identify the regions in orange, red, yellow and pink with conformers  $\alpha_R$ ,  $\alpha_L$ ,  $C_{7ax}$  and  $C_{7eq}$  respectively [39, 46]. Besides, region green corresponds to conformer  $C_5$  and the blue one to  $\alpha'$  [16, 46]. Remarkably, the basin  $\alpha_L$  (one of the less populated state) has been visited 1155 times with a mean stay time of 4.20 ps.

We now look at the coarse-grained picture of the FEL by describing the properties of the 6 basins detected. The different weights of the basins are related to the free energy of the corresponding conformational macro-states. In Table 1 these energy differences  $\Delta F_a = -k_B T \log(P_a/P_{C_{7eq}})$  are shown, taking the most populated basin as the energy reference  $F_{C_{7eq}} = 0$ . The lowest free energy basins correspond to configurations with  $\phi \leq 0^\circ$  ( $C_{7eq}$ ,  $\alpha_R$ ,  $C_5$  and  $\alpha'$ ), whereas the two other conformers located in the region  $\phi \geq 0^\circ$  have the highest free energy but the largest dwell time. Moreover, we have also analyzed the trapping efficiency of each basin by reporting the mean escape time ( $\Delta t/(1 - P_{aa})$ ) as well in Table 1.

**Table 1. Relative free energies and Mean Escape Time of the basins defined by SSD.**

| Basin      | $F_i - F_{C_{7eq}}$ kcal/mol | Mean Escape Time (ps) |
|------------|------------------------------|-----------------------|
| $C_{7eq}$  | 0.00                         | 0.52                  |
| $\alpha_R$ | 0.45                         | 0.42                  |
| $\alpha_L$ | 2.42                         | 4.20                  |
| $C_{7ax}$  | 3.84                         | 0.71                  |
| $C_5$      | 0.55                         | 0.28                  |
| $\alpha'$  | 0.90                         | 0.23                  |

**Table 2. Characteristic times for direct inter-basins transitions.**

| $a \rightarrow b$              | $1/k_{ba}$ (ps) |                                |        |
|--------------------------------|-----------------|--------------------------------|--------|
| $C_{7eq} \rightarrow \alpha_L$ | 1968.34         | $\alpha_L \rightarrow C_{7eq}$ | 88.24  |
| $\alpha_R \rightarrow C_{7ax}$ | 58011.74        | $C_{7ax} \rightarrow \alpha_R$ | 815.87 |
| $C_5 \rightarrow C_{7ax}$      | 393.75          | $C_{7ax} \rightarrow C_5$      | 6.63   |
| $\alpha' \rightarrow \alpha_L$ | 400.57          | $\alpha_L \rightarrow \alpha'$ | 58.47  |
| $C_{7eq} \rightarrow \alpha_R$ | 3.32            | $\alpha_R \rightarrow C_{7eq}$ | 1.88   |
| $\alpha_L \rightarrow C_{7ax}$ | 4.80            | $C_{7ax} \rightarrow \alpha_L$ | 0.78   |

The FEL can be represented as a dendrogram, see Figure 4, where the hierarchical map of the conformers based on Free Energy gives at first glance a global picture of the landscape. Remarkably, the conformer  $\alpha_L$ , despite of having one of the highest free energy, looks like the metastable state with longest life. This result is supported by the values of Mean Escape Time shown in Table 1.

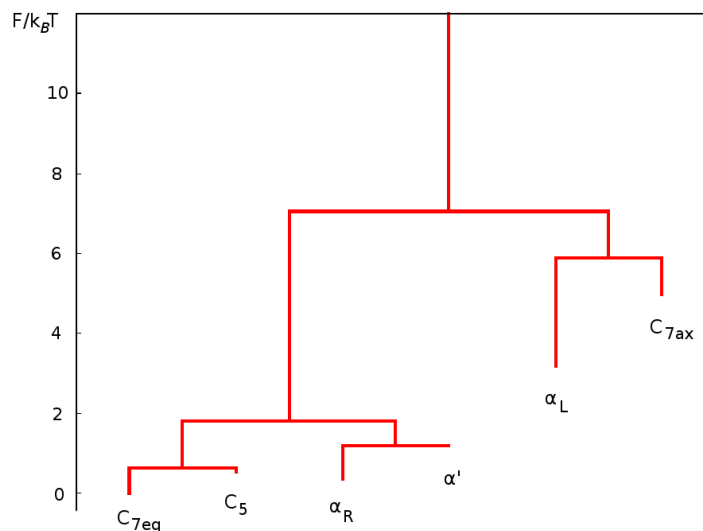


**Figure 4. Dendrogram based on the relative Free Energy of the CMN nodes.** Two sets of basins are clearly distinguished with a high free energy barrier in between:  $(C_{7eq}, \alpha_R, C_5, \alpha')$  and  $(C_{7ax}, \alpha_L)$ . Note that  $\alpha_L$  looks like the conformer with the largest dwell time, in agreement with data in Table 1.

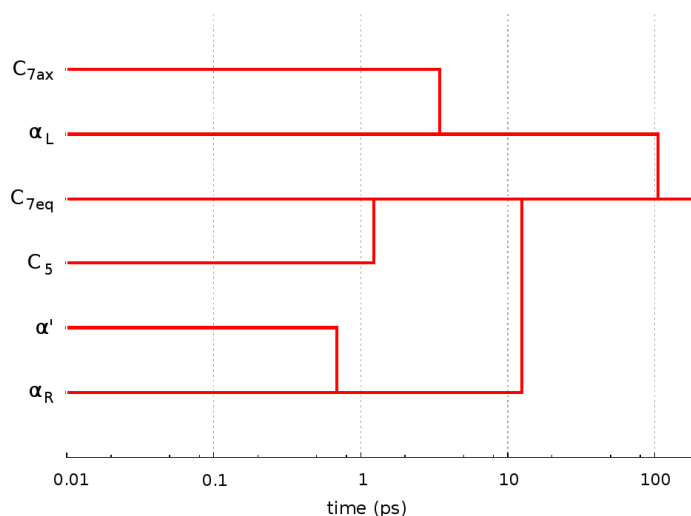


**Figure 5. Dendrogram based on the temporal hierarchy of basins.** In around 100 ps the peptide finds the way to reach the global minimum, conformer  $C_{7eq}$ , from any basin.

The alanine dipeptide has been also studied because of its "fast" isomerization  $C_{7eq} \rightarrow \alpha_R$  and a "slow" transition  $\alpha_R \rightarrow C_{7ax}$ . Our coarse-grained picture of the FEL also allows us to extract information about these transitions. In Table 2 we show some of the relevant characteristic transition times from a basin  $a$  to an adjacent basin  $b$ ,  $1/k_{ba}$ . [The whole data is shown in the *SI*.] Transitions between basins with the same sign of  $\phi$  are remarkably faster (*e.g.*  $C_{7eq} \leftrightarrow \alpha_R$  and  $\alpha_L \leftrightarrow C_{7ax}$ ). While slow transitions are observed for those hops crossing the line  $\phi = 0^\circ$  ( $C_{7eq} \rightarrow \alpha_L$  and  $\alpha_R \rightarrow C_{7ax}$ ), showing them as rare events. Instead, the alanine dipeptide finds more easily paths to go to  $\phi \geq 0^\circ$  conformers through  $C_5 \rightarrow C_{7ax}$  and  $\alpha' \rightarrow \alpha_L$  by crossing  $\phi = 180^\circ$ .

To round off the description of the FEL, the dendrogram corresponding to the temporal hierarchy is shown in Figure 5. From the figure, it becomes clear that the behavior of the dialanine depends on the time scale used for its observation. Again, the same two different sets of conformers are distinguished from this hierarchy. Additionally, the global minimum conformer is reached in around 100 ps from any basin.

Finally, the magnitudes computed here for the alanine dipeptide would allow to construct a first-order kinetic model of 6 coupled differential equations as Eq. (6) (assuming equilibrium intra-basin). This model contains the same information as the kinetic model by Chekmarev et al. for the irreversible transfer of population from  $\alpha_R \rightarrow C_{7ax}$  [41].

## Discussion

Hierarchical landscapes characterize the dynamical behavior of proteins, which in turn depends on the relation between the topology of the basins, their transitions paths and the kinetics over energy barriers. The CMN analysis of trajectories generated by MD simulations is a powerful tool to explore complex FELs.

In this article, we have proposed how to deal with a CMN to unveil the structure of the FEL in a straightforward way and with a remarkable efficiency. The analysis presented here is based on the physical concept of basin of attraction, making possible the study of the conformational structure of peptides and the complete characterization of its kinetics. Note that this has been done without the estimation of the volume of each conformational macro-state in the coordinates space and without the 'a priori' knowledge of the saddle points or the transition paths from a local minimum to another.

On the other hand, the framework introduced in the article provides us with a quantitative description of the dialanine's FEL, coming up directly from a MD dynamics at certain temperature. The peptide explores its landscape building the corresponding CMN and the success of extracting the relevant information is up to the ability of dealing with it. Neither the FE basins were defined by the unique criterion of clustering conformations with a geometrical distance [47], nor the rate constants were projected from the potential energy surface [19, 20]. Moreover, the conformers and their properties were computed from the MD with the only limitation of the discretization of time and space.

Although we have applied the method to low dimensional landscapes, we expect that high dimensional systems could be also studied, by the combination of this technique with the usual methods to reduce the effective degrees of freedom (like principal component analysis or essential dynamics). In conclusion, the large amount of information obtained by working with the CMN, its potential application to any peptide with a large number of monomers, and the possibility of performing the analysis on top of CMN constructed via several short MD simulations [48], make the approach presented here a promising way to describe the FEL of a protein.

## Acknowledgments

A critical reading of the manuscript by Y. Moreno and L.M. Floría, and the helpful comments and suggestions from the anonymous referees are gratefully acknowledged.

## References

1. Oltvai ZN, Barabási AL (2002) Systems biology. Life's complexity pyramid. *Science* 298: 763–764.
2. Parisi G (1994). Complexity in biology: The point of view of a physicist. *arXiv:cond-mat/9412018v1*. Available: <http://arxiv.org/abs/cs/0702048v1>. Accessed 5 December 1994.
3. Krivov SV, Karplus M (2002) Free energy disconnectivity graphs: Application to peptide models. *J Chem Phys* 117: 10894–10903.
4. Krivov SV, Karplus M (2004) Hidden complexity of free energy surfaces for peptide (protein) folding. *Proc Natl Acad Sci U S A* 101: 14766–14770.
5. Ottino JM (2003) Complex systems. *AIChE J* 49: 292–299.
6. Amaral LAN, Ottino JM (2004) Complex systems and networks: challenges and opportunities for chemical and biological engineers. *Chem Eng Sci* 59: 1653–1666.
7. Newman MEJ (2003) The structure and function of complex networks. *SIAM Rev* 45: 167–256.
8. Boccaletti S, Latora V, Moreno Y, Chavez M, Hwang DU (2006) Complex networks: Structure and dynamics. *Phys Rep* 424: 175–308.
9. Noé F, Horenko I, Schütte C, Smith JC (2007) Hierarchical analysis of conformational dynamics in biomolecules: Transition networks of metastable states. *J Chem Phys* 126: 155102-1–155102-17.
10. Rao F, Caffisch A (2004) The protein folding network. *J Mol Biol* 342: 299–306.
11. Caffisch A (2006) Network and graph analyses of folding free energy surfaces. *Curr Opin Struct Biol* 16: 71–78.
12. Noé F, Fischer S (2008) Transition networks for modeling the kinetics of conformational change in macromolecules. *Curr Opin Struct Biol* 18: 154–162.
13. Scala A, Amaral LAN, Barthélémy M (2001) Small-world networks and the conformation space of a short lattice polymer chain. *Europhys Lett* 55: 594–600.
14. Gfeller D, De Lachapelle DM, De los Rios P, Caldarelli G, Rao F (2007) Uncovering the topology of configuration space networks. *Phys Rev E* 76: 026113-1–026113-9.
15. Gfeller D, De Los Rios P, Caffisch A, Rao F (2007) From the cover: Complex network analysis of free-energy landscapes. *Proc Natl Acad Sci U S A* 104: 1817–1822.
16. Chodera JD, Singhal N, Pande VS, Dill KA, Swope WC (2007) Automatic discovery of metastable states for the construction of markov models of macromolecular conformational dynamics. *J Chem Phys* 126: 155101-1–155101-17.
17. Buchete NV, Hummer G (2008) Coarse master equations for peptide folding dynamics. *J Phys Chem B* 112: 6057–6069.

18. Deuffhard P, Huisinga W, Fischer A, Schütte C (2000) Identification of almost invariant aggregates in reversible nearly uncoupled markov chains. *Linear Algebra Appl* 315: 39–59.
19. Wales DJ (2006) Energy landscapes: calculating pathways and rates. *Int Rev Phys Chem* 25: 237–282.
20. Evans DA, Wales DJ (2003) The free energy landscape and dynamics of met-enkephalin. *J Chem Phys* 119: 9947–9955.
21. Wales DJ, Doye JPK, Miller MA, Mortenson PN, Walsh TR (2000) Energy landscapes: From clusters to biomolecules. *Adv Chem Phys* 115: 1–111.
22. Hänggi P, Talkner P, Borkovec M (1990) Reaction-rate theory: fifty years after kramers. *Rev Mod Phys* 62: 251–342.
23. van Kampen NG (2007) *Stochastic Processes in Physics and Chemistry*. North Holland, Third Edition, 463 pp.
24. van Kampen NG (1998) Remarks on non-Markov processes. *Braz J Phys* 28: 90–96.
25. Zwanzig R (2001) *Nonequilibrium Statistical Mechanics*. Oxford University Press, USA, 222 pp.
26. Jernigan RW, Baran RH (2003) Testing lumpability in Markov chains. *Statist Probab Lett* 64: 17–23.
27. Swope WC, Pitera JW, Suits F (2004) Describing protein folding kinetics by molecular dynamics simulations. 1. theory. *J Phys Chem B* 108: 6571–6581.
28. Zwanzig R (1983) From classical dynamics to continuous time random walks. *J Statist Phys* 30: 255–262.
29. Park S, Pande VS (2006) Validation of Markov state models using Shannon’s entropy. *J Chem Phys* 124: 054118-1–054118-5.
30. Wolynes PG, Onuchic JN, Thirumalai D (1995) Navigating the folding routes. *Science* 267: 1619–1620.
31. Onuchic JN, Wolynes PG (2004) Theory of protein folding. *Curr Opin Struct Biol* 14: 70–75.
32. Greenside HS, Helfand E (1981) Numerical integration of stochastic differential equations.2. *Bell Syst Tech J* 60: 1927–1940.
33. If the max value of  $P_{j,l}$  is reached for several neighbors of  $l$  (degeneracy), we choose at random one of them.
34. Danon L, Díaz-Guilera A, Duch J, Arenas A (2005) Comparing community structure identification. *J Stat Mech* 9: P09008-1–P09008-10.
35. Trygubenko SA, Wales DJ (2006) Graph transformation method for calculating waiting times in Markov chains. *J Chem Phys* 124: 234110-1–234110-16.
36. Hoshen J, Kopelman R (1976) Percolation and cluster distribution. 1. Cluster multiple labeling technique and critical concentration algorithm. *Phys Rev B* 14: 3438–3445.
37. Lyman E, Zuckerman DM (2007) On the structural convergence of biomolecular simulations by determination of the effective sample size. *J Phys Chem B* 111: 12876–12882.



38. Rossky PJ, Karplus M (1979) Solvation - molecular dynamics study of a dipeptide in water. *J Am Chem Soc* 101: 1913–1937.
39. Smith PE (1999) The alanine dipeptide free energy surface in solution. *J Chem Phys* 111: 5568–5579.
40. Apostolakis J, Ferrara P, Caffisch A (1999) Calculation of conformational transitions and barriers in solvated systems: Application to the alanine dipeptide in water. *J Chem Phys* 110: 2099–2108.
41. Chekmarev DS, Ishida T, Levy RM (2004) Long-time conformational transitions of alanine dipeptide in aqueous solution: Continuous and discrete-state kinetic models. *J Phys Chem B* 108: 19487–19495.
42. Bolhuis PG, Dellago C, Chandler D (2000) Reaction coordinates of biomolecular isomerization. *Proc Natl Acad Sci U S A* 97: 5877–5882.
43. Hummer G, Kevrekidis IG (2003) Coarse molecular dynamics of a peptide fragment: Free energy, kinetics, and long-time dynamics computations. *J Chem Phys* 118: 10762–10773.
44. Ma A, Dinner AR (2005) Automatic method for identifying reaction coordinates in complex systems. *J Phys Chem B* 109: 6769–6779.
45. Vargas R, Garza J, Hay BP, Dixon DA (2002) Conformational study of the alanine dipeptide at the MP2 and DFT levels. *J Phys Chem A* 106: 3213–3218.
46. Roterman IK, Lambert MH, Gibson KD, Scheraga HA (1989) A comparison of the CHARMM, AMBER and ECEPP potentials for peptides. II. Phi-psi maps for N-acetyl alanine N'-methyl amide: comparisons, contrasts and simple experimental tests. *J Biomol Struct Dyn* 7: 421–453.
47. Becker OM (1997) Geometric versus topological clustering: an insight into conformation mapping. *Proteins* 27: 213–226.
48. Chodera JD, Swope WC, Pitera JW, Dill KA (2006) Long-time protein folding dynamics from short-time molecular dynamics simulations. *Multiscale Model Simul* 5: 1214–1226.

# Supporting Information

## 1 Checking Markovity

Although the purpose of the work introduced in the manuscript was to illustrate a way to handle the Conformational Markov Network (CMN) in order to obtain the basins of attraction and characterize the Free Energy Landscape, the lector must be advise about the necessity of checking the markovian character of the model (network in our case).

With regard to the CMNs that appear in the manuscript:

(i) The particle in the *funnel like potential* is simulated using an overdamped dynamics. In this case, the continuous trajectory integrated is inherently Markovian [1, 2]. When we discretize the coordinate space to lump the trajectory into micro-states, the Markovity of the new description can be defied [3, 4]. Therefore, one has to care about the time step to describe the process since it must be larger than the longest equilibration time among the micro-states [5]. In ref. [6] three approaches are mentioned to evaluate the degree of Markovity of a stochastic model. Among these approaches, we have taken the criterion presented by Park and Pande in [7] based on Shannon’s entropy. This method provides a unique magnitude not as sensitive to statistical and numerical noise as other methods. Another reason to make this choice is that a necessary and sufficient condition for Markovity is checked (while the observation of the eigenvalues of the transition matrix is not a sufficient condition). The analysis is based on the comparison of a first-order conditional entropy  $H_\tau(X_n|X_{n-1})$  and the second-order one  $H_\tau(X_n|X_{n-1}, X_{n-2})$  (see [7] for further details and notation). The magnitude  $R_\tau$  quantifies, given  $X_{n-1}$ , what fraction of the information in  $X_n$  is the mutual information between  $X_n$  and  $X_{n-2}$ . Although the method is computationally expensive, our models are small enough to carry out this analysis. The Figure 6 reveals that with the lag time used in our analysis ( $\tau = 1$ ) the memory effect (non-Markovity) is less than a 5%.

We have to remark, as it is discussed in ref. [7], that there’s probably no answer to the question: when does the model behaves Markovian? However the appropriate question should be: Given an observable, what is the degree of Markovity needed to have a correct measure? Regarding to our work, note that the analysis of the basins detection depends on the detailed balance condition, but not on the relaxation times. On the other hand, a small deviation such as the 5%, only affects at the analysis of the temporal hierarchy of basins, where Chapman-Kolmogorov is used explicitly. In order to distinguish whether the error is propagated (and increased) or not when the transition matrix is raised to the power of  $n$ , we compute the Kullback-Leibler divergence between the transition matrix  $S(\tau)^n$  and the matrix computed from the trajectory  $S(n\tau)$ :

$$D_{KL}(S(n\tau)||S(\tau)^n) = \sum_{ij} S(n\tau)_{ij} P_j \ln \frac{S(n\tau)_{ij}}{[S(\tau)^n]_{ij}}$$

The Figure 7 reveals that the error in the transitions computed with Chapman-Kolmogorov are far from the experimental values during a short range of  $n\tau$  close to the original lag time, but the divergence decrease with time after few steps. In the limit  $n \rightarrow \infty$ , the matrix obtained must be equal to the

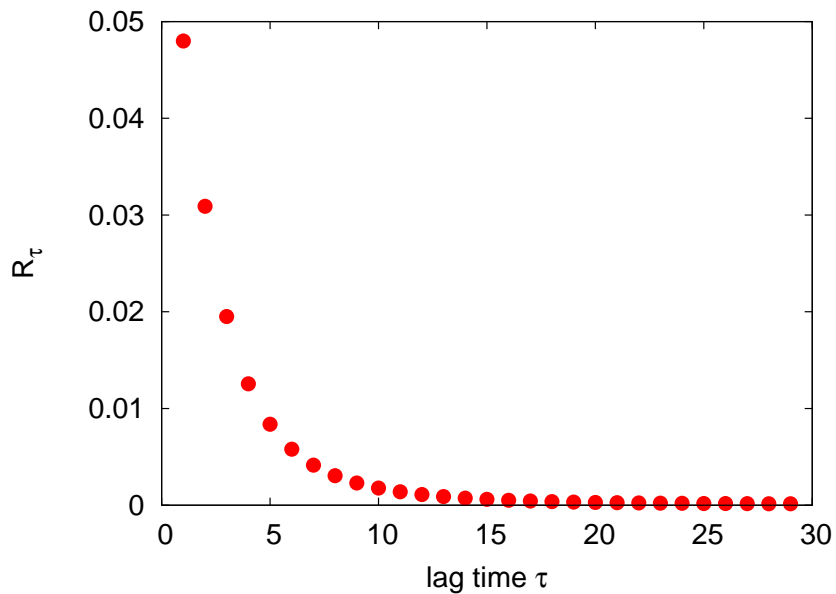


**Figure 6.** Checking Markovity: The relative mutual information  $R_\tau$  quantifies the degree of non-Markovity of our stochastic model. The lag time used to construct the CMN -funnel like potential-,  $\tau = 1$ , reveals a memory effect lower than a 5%.

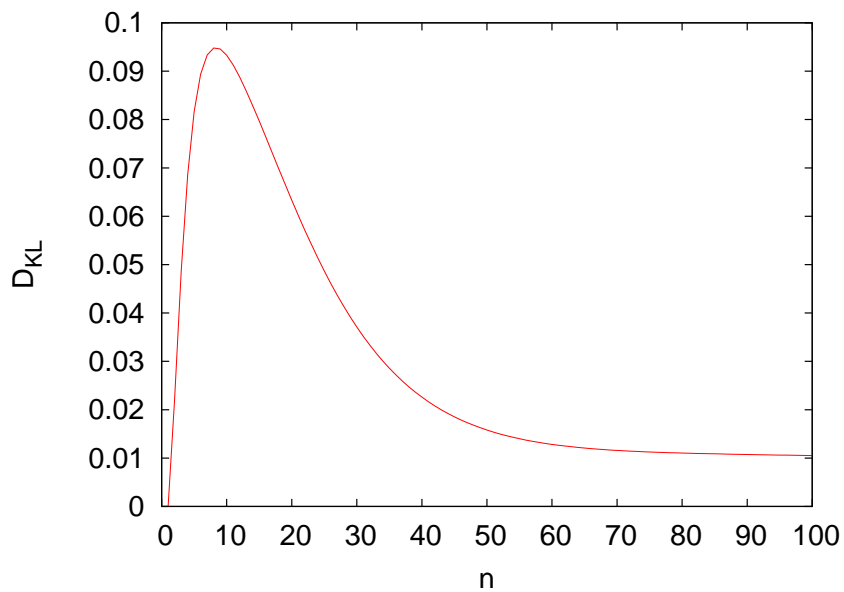


**Figure 7.** The Kullback-Leibler divergence between the "experimental" transition matrix  $S(n\tau)$  and  $S(\tau)^n$  decreases after few time steps ( $\tau$ ).

experimental one (having the stationary probability distribution in each column of the transition matrix).

(ii) The *alanine dipeptide* is simulated with the Langevin formalism (see details in the manuscript and in the *SI*). The continuum trajectory in the space of coordinates and momenta is also inherently Markovian [1,2]. On the other hand, we are integrating momenta and discretizing the coordinates space in our description, which can result in a non-Markovian chain depending on the time step used. In our case the same analysis applied before provides a value of 0.8% of memory effect.

## 2 Comparing with other community algorithms

As it was introduced in the paper, one may be tempted to apply standard algorithms for community detection in complex networks to the problem of unveiling the topology of free energy landscapes. Several authors have made use of current community detection tools [8–13] with diverse degree of success. However, there is no clear conclusion about what method is the most suitable for the problem [14]. Here we sketch the results obtained using two different approaches [12,15] to the community detection that have already been used in previous related works. These results show that our method outperforms any of the proposed algorithms both in the computational complexity and the success in relating the CMN structure to the FEL.

### 2.1 Maximization of Modularity

A number of community detection algorithms have been introduced in the last years making use of the idea of modularity [11,13]. The idea is to find a network partition into disconnected clusters so that a given function, the modularity of the network partition, is maximal. The modularity of a given partition accounts for the probability of having edges connecting nodes belonging to the same cluster in the network minus the expected probability in a randomized version of the network (having the same number of nodes and edges and preserving the strength of the nodes). Therefore, modularity provide a way to quantify the quality of a given network partition, *i.e.* the larger the modularity the better the partitioning is.

The modularity,  $Q$ , for weighted and directed networks has been introduced in ref. [15,16] and, applied to our CMN, it takes the following form:

$$Q = \sum_{ij} [P_i P_{ji} - P_i P_j] \delta(c_i, c_j) \quad (8)$$

where the function  $\delta(x, y)$  is the Kronecker delta function that takes value 1 if  $x = y$  and 0 otherwise. The label  $c_i$  accounts for the community where node  $i$  is assigned in the network partition.

A number of optimization algorithms have been used to look for maximal modularity partitions. We have chosen the spectral decomposition introduced in ref. [15] and a deterministic greedy search algorithm [17,18] to compare with the results obtained for the funnel-like CMN using the *SSD* algorithm. With these two methods we have obtained two optimal partitions of the CMN having  $Q_{max} = 0.54$  and  $Q_{max} = 0.53$  respectively. On the other hand, the modularity value for the basins detected by *SSD* only reaches a value  $Q = 0.116$ . This would seem a bad test for the *SSD*, however, as it is also shown in ref. [14], the community structure obtained by modularity-based methods is far from the basins shown in Figure 1C of *main text*. The most approximated decomposition is obtained by the greedy search algorithm where 11 communities were detected. In this case the most populated basin detected for the funnel-like potential, the basin called *a* in Figure 1C of *main text*, was split in 5 different communities.

This check was not so unwise if one observes that  $Q$  is related with the relaxation times of a stochastic Markov chain represented by the matrix  $\mathbf{S}$  in the article:

$$Q = \sum_{\alpha} \sum_{k \neq 1} (\tau_k + 1) \left( \sum_{i \in \alpha} \xi_i^k \right)^2, \quad (9)$$

where  $\alpha$  is the community index,  $i$  is the node index, and  $\tau_k$  and  $\xi_i^k$  are the eigenvalues -relaxation times- and eigenvectors -relaxation modes- of the stochastic matrix  $\mathbf{M} = \mathbf{S} - \mathbf{1}$ .

Despite of the possible interpretation of communities based on modularity in CMNs, the  $Q$  value obtained for the *SSD* basins is quite farway from being the maximum.

## 2.2 Markov Clustering algorithm

Alternatively to the use of modularity optimization approaches, a second type of algorithms based on random walks has been introduced to infer the structure of complex networks. The most interesting algorithm of this type is the Markov Clustering (MCL) approach [12] since it has been proved to be the best suited method for detecting basins in CMNs [14]. MCL starts with the stochastic matrix  $\mathbf{S}$  and iteratively alternates sequences of two matrix operations (namely expansion and inflation) until the convergence to an invariant matrix (from which network partition is finally obtained) is achieved. Expansion and inflation transformations correspond to matrix squaring and matrix Hadamard  $p$ -power respectively. These two operations are followed to a normalization step to assure that the resulting matrix is stochastic at the end of each iteration. The detected network partition depends crucially on the choice of the parameter  $p \geq 1$ , often called granularity. For its minimum value  $p = 1$  only one community is detected, the whole network. Therefore, the success on finding the right network community structure is achieved by a fine tuning of  $p$ .

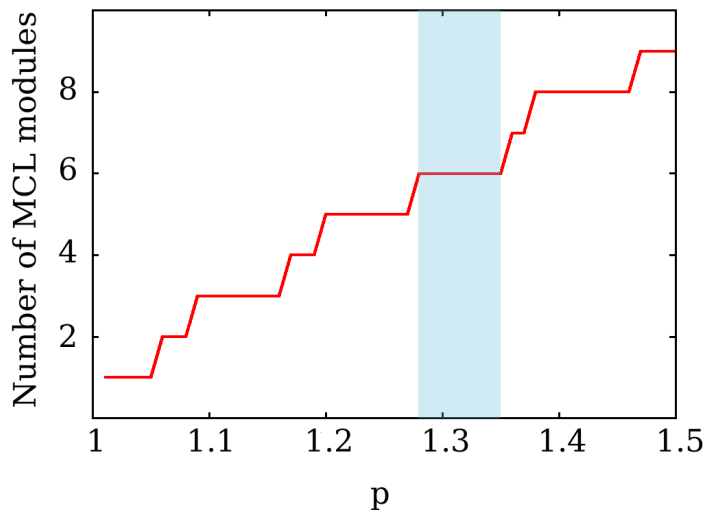


**Figure 8.** Markov Clustering algorithm applied to the funnel-like potential. The figure shows the number of network clusters found by MCL as a function of the granularity parameter  $p$ . As it is shown there is a range of granularity values for which MCL is able to detect the same number of clusters as the *SSD* algorithm.

We have performed the MCL algorithm over the CMN of the funnel-like network, see Figure 8. Unlike modularity-based algorithms, the MCL analysis points out that the network is divided into six communities (basins) for a small range of  $p$ ,  $1.28 \leq p \leq 1.35$  ( $1.5 \leq p < 2.0$  is recommended in the

literature), in agreement with the partition found using the *SSD* algorithm (see Table 3). However, the non-deterministic character of the method would tempt, if we do not have prior knowledge about the structure of the FEL, to evaluate the quality of the partitions by computing their modularity. This would lead us to a CMN partition in disagreement with the number of basins present in the FEL. Therefore, the free parameter  $p$  makes this algorithm unsuitable for analyzing general CMNs since one should have enough prior knowledge about the system to distinguish the best  $p$  value.

**Table 3.** The number of nodes of *SSD* basins are compared with those of the *MCL* modules ( $p = 1.3$ ) for the funnel-like potential.

|            |   | MCL Modules |    |    |    |    |    |
|------------|---|-------------|----|----|----|----|----|
|            |   | 1           | 2  | 3  | 4  | 5  | 6  |
| SSD Basins | a | 56          | 3  |    |    |    |    |
|            | b |             | 29 |    |    |    |    |
|            | c |             |    | 54 |    |    |    |
|            | d |             |    |    | 24 |    |    |
|            | e |             |    |    | 1  | 49 |    |
|            | f |             |    |    |    |    | 25 |

Finally, let us remark that both modularity optimization and *MCL* are computationally far more complex than the *SSD* algorithm. In particular, the modularity optimization scales as  $\mathcal{O}(N^3)$  for the spectral decomposition and as  $\mathcal{O}(mN)$  when greedy algorithm is implemented. On the other hand, *MCL* has a time complexity  $\mathcal{O}(N^3)$ . To our knowledge the unique community detection algorithm that scales linearly in time (specifically as  $\mathcal{O}(L + N)$ ) (with  $L$  being the number of links in the network) was proposed in ref. [19]. However, this latter method assumes a prior knowledge of the number of network clusters and, moreover, these cluster have to be of equal size. As a conclusion, the comparison between *SSD* algorithm and standard community detection [20] methods yields a positive assessment on the convenience of using *SSD* based both on its better performance and linear time complexity. This makes the use of the ‘‘Stochastic steepest descent’’ technique the most appropriate method for analyzing molecular dynamics data from systems of many degrees of freedom such as proteins.

## 3 Alanine dipeptide

### 3.1 Molecular dynamics simulation

The terminally blocked alanine peptide Ace-Ala-Nme has been modeled by the OPLS force field [21] with the program Gromacs 3.3.1 [22] and solvated with TIP4P waters [23]. A Langevin MD simulation has been performed at 400K with a friction coefficient of  $5 \text{ ps}^{-1}$ . In order to set up the CMN, a single trajectory of 250 ns has been analyzed with conformations saved every 0.01 ps (5 MD steps).

### 3.2 Direct inter-basins transitions

An extension of Table 2 of main text is shown with the whole data for the direct transitions.



**Table 4.** Characteristic times for direct transition inter-basins.

| $a \rightarrow b$              | $1/k_{ba}$ (ps) |                                |         |
|--------------------------------|-----------------|--------------------------------|---------|
| $C_{7eq} \rightarrow C_5$      | 0.66            | $\alpha' \rightarrow C_5$      | 1.35    |
| $C_{7eq} \rightarrow \alpha_R$ | 3.32            | $\alpha' \rightarrow C_{7eq}$  | 3.48    |
| $C_{7eq} \rightarrow \alpha'$  | 10.80           | $\alpha' \rightarrow \alpha_R$ | 0.30    |
| $C_{7eq} \rightarrow \alpha_L$ | 1968.34         | $\alpha' \rightarrow \alpha_L$ | 400.57  |
| $C_5 \rightarrow C_{7eq}$      | 0.33            | $C_{7ax} \rightarrow C_5$      | 6.63    |
| $C_5 \rightarrow \alpha_R$     | 98.25           | $C_{7ax} \rightarrow \alpha_R$ | 815.87  |
| $C_5 \rightarrow \alpha'$      | 2.11            | $C_{7ax} \rightarrow \alpha_L$ | 0.78    |
| $C_5 \rightarrow C_{7ax}$      | 393.75          | $\alpha_L \rightarrow C_5$     | 1213.40 |
| $C_5 \rightarrow \alpha_L$     | 51187.87        | $\alpha_L \rightarrow C_{7eq}$ | 88.24   |
| $\alpha_R \rightarrow C_5$     | 110.28          | $\alpha_L \rightarrow \alpha'$ | 58.47   |
| $\alpha_R \rightarrow C_{7eq}$ | 1.88            | $\alpha_L \rightarrow C_{7ax}$ | 4.80    |
| $\alpha_R \rightarrow \alpha'$ | 0.54            |                                |         |
| $\alpha_R \rightarrow C_{7ax}$ | 58011.74        |                                |         |

## References

1. van Kampen NG (1998) Remarks on non-Markov processes. *Braz J Phys* 28: 90–96.
2. Zwanzig R (2001) *Nonequilibrium Statistical Mechanics*. Oxford University Press, USA, 222 pp.
3. Huisinga W, Schütte C, Stuart AM (2003) Extracting macroscopic stochastic dynamics: Model problems. *Commun Pure Appl Math* 56: 234–269.
4. Jernigan RW, Baran RH (2003) Testing lumpability in Markov chains. *Statist Probab Lett* 64: 17–23.
5. Swope WC, Pitera JW, Suits F (2004) Describing protein folding kinetics by molecular dynamics simulations. 1. theory. *J Phys Chem B* 108: 6571–6581.
6. Chodera JD, Singhal N, Pande VS, Dill KA, Swope WC (2007) Automatic discovery of metastable states for the construction of markov models of macromolecular conformational dynamics. *J Chem Phys* 126: 155101-1–155101-17.
7. Park S, Pande VS (2006) Validation of Markov state models using Shannon’s entropy. *J Chem Phys* 124: 054118-1–054118-5.
8. Radicchi F, Castellano C, Cecconi F, Loreto V, Parisi D (2004) Defining and identifying communities in networks. *Proc Natl Acad Sci U S A* 101: 2658–2663.
9. Donetti L, Muñoz MA (2004) Detecting network communities: a new systematic and efficient algorithm. *J Stat Mech* 2004: P10012-1–P10012-15.
10. Girvan M, Newman MEJ (2002) Community structure in social and biological networks. *Proc Natl Acad Sci U S A* 99: 7821–7826.
11. Newman MEJ, Girvan M (2004) Finding and evaluating community structure in networks. *Phys Rev E* 69: 026113-1–026113-15.
12. van Dongen SM (2000) *Graph Clustering by Flow Simulation*. Ph.D. thesis, University of Utrecht, The Netherlands.

13. Newman MEJ (2006) From the cover: Modularity and community structure in networks. *Proc Natl Acad Sci U S A* 103: 8577–8582.
14. Gfeller D, De Los Rios P, Caffisch A, Rao F (2007) From the cover: Complex network analysis of free-energy landscapes. *Proc Natl Acad Sci U S A* 104: 1817–1822.
15. Leicht EA, Newman MEJ (2008) Community structure in directed networks. *Phys Rev Lett* 100: 118703-1–118703-4.
16. Newman MEJ (2004) Analysis of weighted networks. *Phys Rev E* 70: 056131-1–056131-9.
17. Newman MEJ (2004) Fast algorithm for detecting community structure in networks. *Phys Rev E* 69: 066133-1–066133-5.
18. Wakita K, Tsurumi T (2007) Finding community structure in mega-scale social networks. *arXiv:cs/0702048v1* Available: <http://arxiv.org/abs/cs/0702048v1>. Accessed 8 February 2007.
19. Wu F, Huberman B (2004) Finding communities in linear time: a physics approach. *Eur Phys J B* 38: 331–338.
20. Danon L, Díaz-Guilera A, Duch J, Arenas A (2005) Comparing community structure identification. *J Stat Mech* 9: P09008-1–P09008-10.
21. Jorgensen WL, Maxwell DS, Tirado-Rives J (1996) Development and testing of the opls all-atom force field on conformational energetics and properties of organic liquids. *J Am Chem Soc* 118: 11225–11236.
22. Van Der Spoel D, Lindahl E, Hess B, Groenhof G, Mark AE, et al. (2005) Gromacs: fast, flexible, and free. *J Comput Chem* 26: 1701–1718.
23. Jorgensen WL, Chandrasekhar J, Madura JD, Impey RW, Klein ML (1983) Comparison of simple potential functions for simulating liquid water. *J Chem Phys* 79: 926–935.